

Probing Environmental Spin Polarization with Superconducting Flux Qubits

T. Lanting,¹ M. H. Amin^{†,1,2} C. Baron,¹ M. Babcock,¹ J. Boschee,³
S. Boixo,⁴ V. N. Smelyanskiy,⁴ M. Foygel,⁵ and A. G. Petukhov⁶

¹*D-Wave Systems Inc., 3033 Beta Avenue, Burnaby, British Columbia V5G 4M9, Canada*

²*Department of Physics, Simon Fraser University, Burnaby BC, Canada, V5A 1S6*

³*Department of ARC, University of British Columbia, Vancouver, British Columbia V6T 1Z3, Canada*

⁴*Google Inc., Venice, California 90291, USA*

⁵*SGT, Inc., NASA Ames Research Center, Moffett Field, California 94035, USA*

⁶*Google Inc., Santa Barbara, California 93117, USA*

(Dated: April 2, 2020)

We present measurements of the dynamics of a polarized magnetic environment coupled to the flux degree of freedom of rf-SQUID flux qubits. The qubits are used as both sources of polarizing field and detectors of the environmental polarization. We probe dynamics at timescales from $5 \mu\text{s}$ to 5ms and at temperatures between 12.5 and 22mK . The measured polarization versus temperature provides strong evidence for a phase transition at a temperature of $5.7 \pm 0.3 \text{mK}$. Furthermore, the environmental polarization grows initially as \sqrt{t} , consistent with spin diffusion dynamics. However, spin diffusion model deviates from data at long timescales, suggesting that a different phenomenon is responsible for the low-frequency behavior. A simple $1/f$ model can fit the data at all time scales but it requires empirical low- and high-frequency cutoffs. We argue that these results are consistent with an environment comprised of random clusters of spins, with fast spin diffusion dynamics within the clusters and slow fluctuations of the total moments of the clusters.

I. INTRODUCTION

Superconducting qubits are rapidly developing and offer a promising path to a large-scale quantum computing technology [1]. Magnetic flux noise remains a major limitation in these devices and there is an on-going effort to identify and reduce it. Direct experimental measurements reveal a power spectral density that depends on frequency as $1/f^\alpha$ for small f , with $\alpha \lesssim 1$ [2–7]. Despite several decades of investigation, the microscopic origin of such a noise is not well understood, although several theories have been proposed [8–15]. The most likely source of magnetic noise is electron spin defects located in the vicinity of the qubit wiring, specifically in or near the interface between superconducting wiring material and oxide or dielectric layers [6–8, 16]. Moreover, the observed [16] cross-correlation between flux and inductance noise indicates existence of a long-range ferromagnetic order in the spin environment. This observation has led to models based on thermally fluctuating random clusters of spins [12–14]. Spin diffusion is another attractive model that explains some experimental observations [10, 11]. However, spin diffusion does not predict the observed $1/f$ noise spectrum, over a wide range of frequencies. Especially, at frequencies exceeding 1kHz , the dependence is predicted to be $f^{-3/2}$ [11]. These frequencies are typically out of reach for direct flux noise measurements, which become challenging for timescales shorter than 1ms .

The interaction between the magnetic field produced by persistent current flowing in the body of a flux qubit

and the surrounding spin environment offers a powerful new way of probing the dynamical behaviour of this environment at shorter timescales. This persistent current produces a magnetic field that causes a fraction of spins to align. This results in a polarization of the environment, which produces a change in magnetic flux bias that shifts the qubit degeneracy point. By varying the time during which persistent current is either present or absent, we can probe the dynamics of the environmental spin polarization and depolarization.

Here, we present measurements of environmental spin polarization and depolarization for timescales from $5 \mu\text{s}$ to 5ms and for temperatures ranging from $T = 12.5 \text{mK}$ to 22mK . We first describe the detailed protocol used for the experiment and then present fits of the dynamics to candidate models. The fits suggest that a random spin diffusion model works well for describing the short timescale growth that shows a \sqrt{t} dependence, but fails to describe the long-time behaviour. The amplitude of the polarization as a function of environment temperature fits well to a Curie-Weiss model with a phase transition at $5.7 \pm 0.3 \text{mK}$.

II. EXPERIMENT

The qubit design used for these experiments is a compound-compound Josephson junctions (CCJJ) rf-SQUID flux qubit [17]. Two external control bias lines, Φ_q^x and Φ_{CCJJ}^x , shown in Fig. 1(a) allow control of the qubit dynamics and energy landscape. The Hamiltonian of this qubit coupled to a magnetic environment can be written as:

$$\hat{\mathcal{H}} = -\frac{\Delta}{2}\hat{\sigma}_x - \frac{1}{2}(\epsilon + \xi)\hat{\sigma}_z, \quad (1)$$

[†]corresponding author, e-mail: amin@dwavesys.com

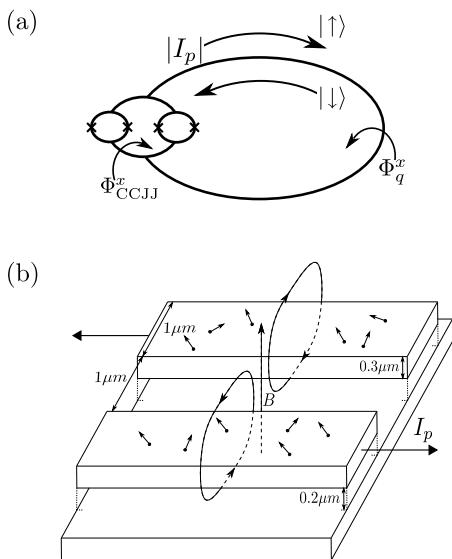


FIG. 1: (a) Schematic of the rf-SQUID flux qubit used in this study. External control biases Φ_{CCJJ}^x and Φ_q^x allow us to adjust parameters Δ , I_p , and ϵ as described in detail in [17]. (b) Cross section of the qubit wiring. The dielectric layer between wiring layers is not shown. Persistent current flowing in the main qubit loop produces a magnetic field that causes a Zeeman splitting of nearby electronic spin defects. At low temperatures, the environmental spins begin aligning with this field.

where $\hat{\sigma}_{z,x}$ are the Pauli matrices, Δ is the tunneling energy, $\epsilon = 2I_p\Phi_q^x$ is the external energy bias, and I_p is the persistent current. The external flux Φ_q^x is measured relative to the degeneracy point, where the two localized states $|\uparrow\rangle$ and $|\downarrow\rangle$ are equally populated. Both I_p and the tunneling energy Δ can be tuned with the external bias Φ_{CCJJ}^x . The potential energy of the rf-SQUID can be made monostable, with zero persistent current flowing in the main body, as well as bistable, with nonzero persistent current. The persistent current applies a polarizing magnetic field to the spins near the surface of the qubit wiring as depicted in Fig. 1(b). We treat the environment as an ensemble of classical spins causing a fluctuating energy bias ξ . Fast random fluctuations of ξ capture the effect of flux noise with a slow drift of the expectation value $\bar{\xi}(t)$ (the order parameter) representing polarization or depolarization of the environment.

To measure the environmental polarization, we use the protocol shown in Fig. 2. We begin by adjusting $\Phi_q^x = 0$ ($\epsilon = 0$) and following a two-part protocol. In the first part, the external bias $\Phi_{\text{CCJJ}}^x = -0.5\Phi_0$ is applied during a recovery time τ_r , making the qubit monostable. At this applied bias, the tunneling energy $\Delta \gg k_B T$ while the persistent current I_p is negligibly small, so the qubit and spin environment are effectively decoupled and each can relax independently. We then initialize the qubit in one of its two localized states, characterized by a persistent current I_p ($\sim 2 \mu\text{A}$). This is done by applying a

preparation bias Φ_q^p while annealing the qubit by changing Φ_{CCJJ}^x to $-1.0\Phi_0$ within anneal time τ_a . The qubit potential barrier then stays high for a polarization time τ_p , with effectively no tunneling between the two bistable states. In this polarization phase, the persistent current in the qubit body generates a magnetic field that partially polarizes the spin environment surrounding the qubit wiring.

After the polarization phase, we measure the environmental polarization using the qubit itself. To do this we first need to get the qubit out of its locked state by lowering its energy barrier. We adjust $\Phi_{\text{CCJJ}}^x = -0.5\Phi_0$ for a short time τ_d , enough for the qubit to lose its memory. Once the barrier is raised again, the qubit will be localized into one of its bistable states depending on the direction of the environmental polarization. The state of the qubit at the end of this anneal is measured and recorded. We apply a feedback flux bias $-\Phi_q^{\text{fb}}$ to the qubit body before raising the potential barrier and tune it so that the qubit is pushed back to its degeneracy. The magnitude of Φ_q^{fb} needed to make the qubit have equal population of both states is a direct measure of the polarization flux. The second part of the protocol in Fig. 2 is a repetition of the first part except the sign of Φ_q^p is reversed. This initializes the qubit in the opposite persistent current state, flipping the direction of the magnetic field polarizing the spin environment, which in turn changes the sign of Φ_q^{fb} . The full protocol is repeated several times and the difference between the results from the two subsequent readouts is recorded. From this feedback signal we can thus directly determine $|\bar{\xi}(t_p)| = 2|I_p\Phi_q^{\text{fb}}|$. Note that with the energy barrier low (monostable), the qubit persistent current vanishes, and the qubit decouples from the spin environment. Thus, during time τ_d the spin polarization starts to relax. To detect the polarization of the spin environment, we typically adjust the protocol such that $\tau_d \ll \tau_p$. For the depolarization measurement, on the other hand, we allow large values τ_d , while keeping τ_p fixed.

We applied the protocol shown in Fig. 2 to flux qubits in a calibrated quantum annealing processor with 2013 working qubits. Typical polarization and depolarization measurements of Φ_q^{fb} at $T = 12.5 \text{ mK}$ are shown in Figs. 3(a) and (b). The symbols show the mean signal across all devices in the processor. For the polarization growth experiment, plotted in Figs. 3(a), τ_p is varied while τ_d is fixed at a small value ($1 \mu\text{s}$). For depolarization measurement, we fix τ_p and measure Φ_q^{fb} as a function of τ_d , as depicted in Fig. 3(b).

III. CANDIDATE MODELS

To understand the data shown in Fig. 3, we need models that relate measurements of Φ_q^{fb} to the dynamics of the ensemble of environmental spins that produces the term ξ in Hamiltonian (1). As we show in Appendix A (see also [18]), linear response theory requires a close rela-

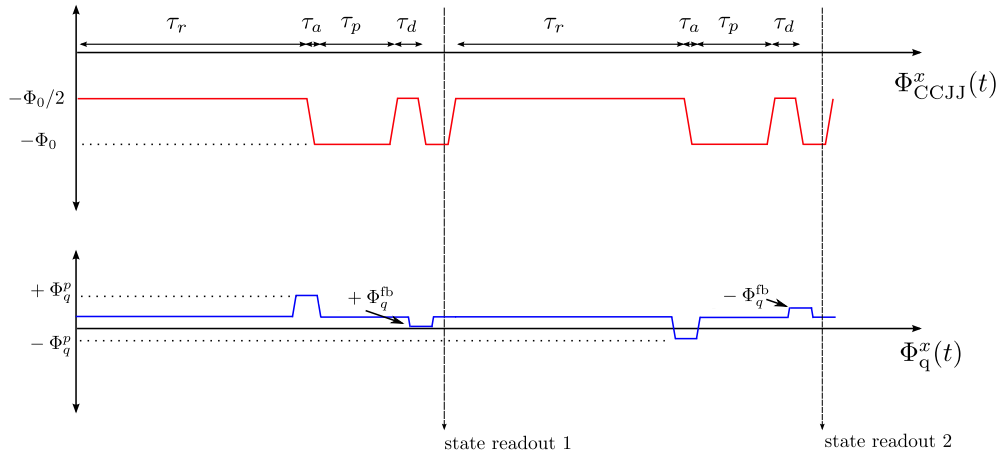


FIG. 2: Experimental protocol for measuring the polarization of the spin environment. We plot the time-dependent external qubit biases, $\Phi_{\text{CCJJ}}^x(t)$ and $\Phi_q^x(t)$ in the top and bottom panels, respectively. Φ_q^x is measured with respect to qubit degeneracy. Two opposite initializations are interleaved to minimize the contribution of low-frequency noise to the measurement. A large ensemble of measurements is performed to determine the feedback signal Φ_q^{fb} necessary to zero population differences between the two initializations. Φ_q^{fb} is thus a direct measurement of the magnitude of the spin environment bias $\bar{\xi}(t)$ on the qubit body.

tion between time-dependent expectation $\bar{\xi}(t)$, i.e., linear response, and the noise spectral density:

$$S_{\Phi}(\omega) = \frac{T}{\omega I_p^2} \int_0^{\infty} dt \sin(\omega t) \left| \frac{d\bar{\xi}(t)}{dt} \right|, \quad (2)$$

where $\omega = 2\pi f$ is the angular frequency.

In the absence of coupling between the qubit and the environment, the environmental spins are in a disordered paramagnetic state with zero net magnetization, leading to a zero ensemble average: $\bar{\xi}(t) = 0$. The classical states of the qubit are eigenstates of $\hat{\sigma}_z$. In these states, the qubit applies a polarizing field to the environment. This produces a nonzero average $\bar{\xi}(t)$ that is expected to monotonically increase with time until it saturates at its equilibrium value $\epsilon_p \equiv \bar{\xi}(\infty)$. As soon as the qubit-environment coupling is turned off, the environment starts relaxing back toward $\bar{\xi}(t) = 0$.

To model the experimental data, we consider the general case where the environment polarizes within time τ_p and then depolarizes within time τ_d . In the appendices, we provide detailed derivations for the time dependence of $\bar{\xi}(t)$ based on several underlying models. For all models, we can write the time dependence as

$$\bar{\xi}(\tau_p, \tau_d) = \epsilon_p [F(\tau_d) - F(\tau_d + \tau_p)]. \quad (3)$$

For example, to model a polarization experiment, we set $\tau_d \sim 0$ and vary τ_p , and for depolarization we fix τ_p and study the τ_d dependence of $\bar{\xi}$. The envelope function $F(t)$ captures the time dynamics and depends on the specific model of the spin environment. $F(t)$ has the properties: $F(0) = 1$ and $F(\infty) = 0$. This function fully describes the relaxation behavior and is closely related

to the noise spectral density (see Appendix B) [23]. In the appendices, we consider three different models for the spin environment: homogeneous and inhomogeneous spin diffusion models and a model based on $1/f$ noise spectrum.

For the spin diffusion model, dynamics is governed by random walk in the space of spin configurations, keeping the total magnetization constant. We consider homogeneous and inhomogeneous environments. In the homogeneous case, both the distribution of spins and their coupling are assumed to be uniform. In the inhomogeneous case, on the other hand, we assume spins form clusters of random sizes with strong spin-spin interaction within each cluster. Both models are shown to have asymptotic behavior for short and long times given by (see Appendix D)

$$F(t) = \begin{cases} 1 - C\sqrt{\Omega t} & \text{for } t \ll \Omega^{-1} \\ C'e^{-\kappa(\Omega t)^\nu} & \text{for } t \gg \Omega^{-1} \end{cases}, \quad (4)$$

where C and C' are model dependent coefficients and $\kappa = 4(3)$ and $\nu = 1(1/3)$ for the homogeneous (inhomogeneous) case. The parameter Ω^{-1} is the timescale over which the magnetization can diffuse freely before encountering the geometric boundaries of either the qubit wiring (the homogeneous case) or the clusters (the inhomogeneous case). Notice that in both cases, the short time environmental polarization has the \sqrt{t} dependence expected for random walk. This dependence is associated with asymptotic $f^{-3/2}$ behavior of the noise spectral density through Eq. (2). At long times, on the other hand, the decay is exponential in the homogeneous case and stretched-exponential in the inhomogeneous case. As we

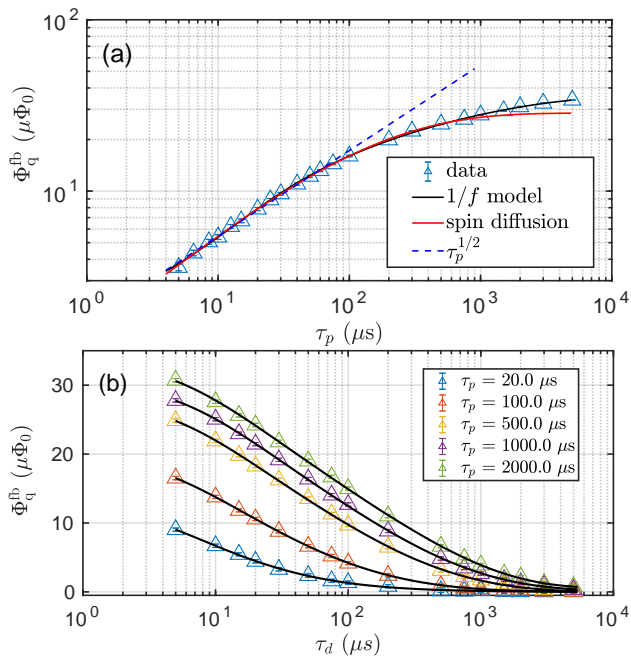


FIG. 3: Measurements of Φ_q^{fb} versus time for (a) polarization and (b) depolarization experiments at $T = 12.5$ mK. In panel (a) τ_d is fixed at $1 \mu\text{s}$. In both panels, the solid black curves show best fits to Eq. (7) assuming dynamics governed by the empirical model given by Eq. (5). The dashed line in (a) represents $\sqrt{\tau_p}$ -dependence and the solid red curve is obtained from spin diffusion model (Eq. (D12)) as described in the text.

shall see in the next section, while the short-time behavior agrees very well with \sqrt{t} -dependence, both the exponential or the stretched-exponential decays predict the polarization to saturate at long timescales faster than what is observed experimentally.

We also consider an empirical model for the spin environment assuming a noise power spectral density $S_\Phi(f) = A/f^\alpha$, consistent with direct low-frequency observations [11]. We assert a short and long time cut-offs, τ_{min} and τ_{max} such that $S(f < 1/2\pi\tau_{\text{max}}) = 0$ and $S(f > 1/2\pi\tau_{\text{min}}) = 0$. In Appendix C we show that for this model,

$$F(t) = \mathcal{N}t^{\alpha-1}[\Gamma(1-\alpha, t/\tau_{\text{max}}) - \Gamma(1-\alpha, t/\tau_{\text{min}})], \quad (5)$$

where $\Gamma(s, t)$ is the incomplete gamma function and

$$\mathcal{N}^{-1} = \begin{cases} \log(\tau_{\text{max}}/\tau_{\text{min}}) & \alpha = 1 \\ (\alpha-1)^{-1}[\tau_{\text{max}}^{\alpha-1} - \tau_{\text{min}}^{\alpha-1}] & \alpha \neq 1 \end{cases} \quad (6)$$

is a normalization factor. Note that Eq. (5) has three fitting parameters ($\alpha, \tau_{\text{min}}, \tau_{\text{max}}$) in contrast to one (Ω) in the spin diffusion model. In the next section, we explore how these theoretical models fit the experimental data.

IV. DATA ANALYSIS

To fit our experimental data, we express Eq. (3) directly in terms of flux

$$\Phi_q^{\text{fb}}(\tau_p) = \Phi_p[F(\tau_d) - F(\tau_d + \tau_p)], \quad (7)$$

where Φ_q^{fb} is the flux bias applied to the body of the qubit by the polarized spin environment, and $\Phi_p = \epsilon_p/2I_p$ is the equilibrium polarization flux. The dashed blue line in Fig. 3 (a) represents the $\sqrt{\tau_p}$ growth predicted by the short-time limit of the spin diffusion model in Eq. (4). It is clear that the spin diffusion model fits the experimental data for short time scales $\tau_p < 1$ ms. The red solid line in Fig. 3 (a) is obtained by fitting the inhomogeneous spin diffusion model (Eq. (D12)) to experimental data up to $\tau_p = 1$ ms. Since the cutoff point at 1 ms is not well defined, the fitting parameters cannot be accurately determined, but just roughly estimated ($\Phi_p \sim 34 \mu\Phi_0$ and $\Omega \sim 100$ Hz).

At long polarization times, the theoretical curve, which follows the stretched-exponential law of Eq. (4) with $\nu = 1/3$, saturates faster than the experimental data. Trying to fit to the homogeneous spin diffusion model results in an even larger deviation due to the exponential law in Eq. (4) with $\nu = 1$. This suggests that at long times (low frequencies) something beyond spin diffusion is contributing to the flux noise.

Next, we try to fit the data to the empirical $1/f$ based model of Eq. (5). Best fits are plotted as solid curves in Fig. 3(a) and (b). The fitting parameters are: $\Phi_p = 34.8 \pm 0.1 \mu\Phi_0$, $\tau_{\text{min}} = 11.6 \pm 0.1 \mu\text{s}$, and $\tau_{\text{max}} = 8560 \pm 100 \mu\text{s}$ for the polarization curve and $\Phi_p = 35.4 \pm 0.2 \mu\Phi_0$, $\tau_{\text{min}} = 6.3 \pm 0.2 \mu\text{s}$, and $\tau_{\text{max}} = 3470 \pm 5 \mu\text{s}$ for all depolarization curves (averaged over all curves). For all data the best fit $\alpha = 0.98 \pm 0.03$. This model provides a good fit to the experimental data at all timescales, which is not a surprise since it has three fitting parameters; unlike that spin diffusion model that has only one. Nevertheless, the extracted α is close to 1, as expected for $1/f$ noise, and the other fitting parameters are roughly consistent between the polarization curve and all depolarization ones.

We also measured the temperature dependence of the spin environment dynamics by repeating the depolarization experiment at a range of temperatures. Fig. 4(a) shows typical depolarization data for temperatures ranging from 12.5 mK to 21 mK. We also show best fits of the data to Eq. (7) with $F(t)$ defined by Eq. (5). The cutoff parameters τ_{min} and τ_{max} are relatively independent of temperature (Fig. 4(b)), whereas there is a strong temperature dependence on the polarization amplitude $\Phi_p(T)$ (Fig. 4(c)). In Fig. 4(c) we also show a fit of the amplitude versus temperature data to the Curie-Weiss model. The best fit to the Curie-Weiss model estimates critical temperature $T_c = 5.7 \pm 0.3$ mK. The observed proximity to a phase transition is consistent with the previous observation of a T -dependent diffusion coefficient in Ref. [11].

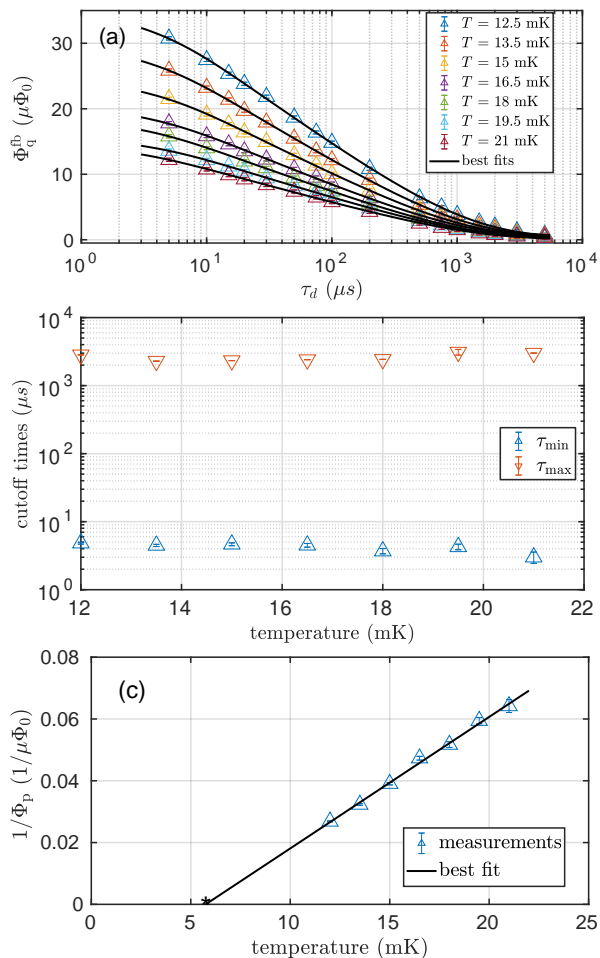


FIG. 4: (a) Measurements of Φ_q^{fb} for a range of temperatures. The data shown are from a protocol that varied τ_d and fixed $\tau_p = 2$ ms. The solid lines show best fits to Eq. (7) using $1/f$ model with parameters $\tau_{\text{min}}(T)$ and $\tau_{\text{max}}(T)$ shown in (b) and $\Phi_p(T)$ shown in (c). From the fit to the Curie-Weiss model, we estimate a critical temperature $T_c = 5.7 \pm 0.3$ mK.

V. DISCUSSION

The experimental results presented here can guide us to a most likely model for flux noise, or at least narrow down the possibilities. Two clear observations stand out that demand explanation: the initial \sqrt{t} growth of the environmental polarization, and the existence of a phase transition at $T_c \approx 5.7$ mK. The former is model independent and the latter, although obtained after a fitting, is insensitive to the model; consistent values of Φ_p were obtained by fitting to different models in Fig. 3. The close proximity to a phase transition shown in Fig. 4 (c) supports theories that allow for long-range ferromagnetic spin ordering. The \sqrt{t} dependence, on the other hand, is a clear indication of a random diffusion process. The spin diffusion model is consistent with both observations and, as we shall show below, provides a quantitatively consistent description of the observed short-time dynamical

behavior above the transition point. Nevertheless, it fails to explain the long-time behavior.

The factor $\Phi_p = \epsilon_p/2|I_p|$ in the polarization/relaxation curves measured in the units of the flux quantum Φ_0 , is identified with the reorganization energy ϵ_p (the spin polaron shift, see Eq. (D24)) and therefore is proportional to the static Curie-Weiss magnetic susceptibility $\chi(T) = n_s \mu_B^2 S(S+1)/3(T - T_c)$, where μ_B is the Bohr magneton, n_s is the 2D concentration of the interface defects with spin S , and T_c is the temperature of ferromagnetic phase transition. For a wire interface of width W , thickness $h \ll W$, and length of the loop, $L \gg W$, the factor Φ_p for spins $S = 1/2$ can be expressed as:

$$\Phi_p(T) \simeq \frac{2(\mu_0 \mu_B)^2 n_s |I_p| L}{W(T - T_c)}, \quad (8)$$

where μ_0 is the magnetic susceptibility of vacuum. From Fig. 4 (c) it is seen that the factor $\Phi_p(T)$ clearly obeys the Curie-Weiss law, so that the system of paramagnetic spins undergoes a ferromagnetic transition at $T_c = 5.7$ mK. Also, with $|I_p| = 2 \mu\text{A}$, $L = 0.7$ mm, and $W = 1 \mu\text{m}$ and with the help of Eq. (8) we can estimate the surface spin density as $n_s = 1.2 \times 10^{12} \text{ cm}^{-2}$ in a reasonable agreement with a previously reported value of 10^{13} cm^{-2} obtained for similar devices [11].

To describe the inhomogeneous spin diffusion, we assume that N_s spins are randomly distributed over a regular lattice of N sites with the filling factor $x_f = N_s/N$. This lattice contains $N_v = N - N_s = N(1 - x_f)$ “vacancies” (i.e., sites where the spin is absent) that terminate spin diffusion. The latter is considered as a process when nonequilibrium magnetization can relax only via angular momentum transfer between spatially close spins due to exchange or dipole-dipole interaction between them. As a result, if the system is below the percolation threshold with respect to the spin sites, the diffusion will be confined within finite clusters comprised of connected nearest-neighbor spin sites that are surrounded by vacancies.

The spin diffusion coefficient \mathcal{D} and the surface spin concentration n_s are related because

$$\mathcal{D} = \eta J a^2, \quad (9)$$

where for a 2D spin environment $a \simeq (x_f/n_s)^{1/2}$ is the distance between the nearest spins along the direction of the magnetic field (see Fig. 1(b)), $\eta = \pi^{1/2}(T - T_c)/2T$ [19]. Here J is the effective strength of the spin-spin coupling, which for the purposes of estimation can be evaluated as interaction energy of two magnetic spin dipoles with $S = 1/2$ [20]:

$$J \simeq \frac{\mu_0 \mu_B^2}{4\pi a^3}. \quad (10)$$

In addition, according to the inhomogeneous spin diffusion model (see Appendix D for details), the diffusion coefficient \mathcal{D} is related to the parameter Ω in Eq. (4) and the

average length of the spin cluster $\bar{w} = n_s^{-1/2}(1 - x_f^{1/2})^{-1}$ as

$$\Omega = \frac{\pi^2 \mathcal{D}}{\bar{w}^2}. \quad (11)$$

Using Eqs. (9)-(11) with the experimentally extracted values $n_s = 1.2 \times 10^{12} \text{ cm}^{-2}$ and $\Omega \simeq 100 \text{ Hz}$ at $T = 12.5 \text{ mK}$, we can estimate the average size of the spin clusters to be $\bar{w} \sim 0.5 \mu\text{m}$ and $\mathcal{D} \simeq 3 \times 10^{-8} \text{ cm}^2/\text{s}$, in agreement with [11]. Note that due to the uncertainties in all parameters, these are very rough estimations. Nevertheless, they show consistency among different quantities within the spin diffusion model.

As is clear from Fig. 3(a), spin diffusion predicts faster long time saturation of polarization than the observed data, meaning that the low-frequency noise must have a different origin. This is consistent with the previous results [11] indicating that spin diffusion does not explain the $1/f^\alpha$ noise dependence over the observed wide frequency range [6, 11]. Fitting the polarization and depolarization data to a model based on $1/f^\alpha$ noise provides a nice agreement at all timescales. However, empirical low- and high-frequency cutoffs are needed to achieve a good fit. The fact that τ_{\min} and τ_{\max} fall within the measured range of τ_p shows that $1/f^\alpha$ spectrum does not hold over the whole range of relevant frequencies. This was indeed expected, especially at large frequencies, since the short-time \sqrt{t} behavior requires asymptotic $f^{-3/2}$ dependence.

To provide a plausible explanation for these observations, we recall that spin diffusion by construction assumes a constant total magnetic moment. This assumption, although valid at short times, is not expected to hold at long times, especially in the presence of dissipation. Slow evolution of the total magnetic moment can produce additional polarization at long times and contribute to the $1/f^\alpha$ noise spectrum at low frequencies. In an inhomogeneous spin environment, the net magnetic moment of each cluster can slowly grow with time or the clusters can slowly align with the external field, in addition to the changes of their internal magnetic distribution governed by spin diffusion. This demands for a theoretical model that describes both fast spin diffusion dynamics and slow fluctuations of total magnetic moments under a unified framework. It should be mentioned that based on our observations, the environment is above, but close to, the critical temperature, and therefore is in paramagnetic phase. This is in contrast to what some spin cluster models of $1/f^\alpha$ noise assume [12–14], hence those theories cannot directly apply here.

VI. CONCLUSION

We have measured the polarization and relaxation dynamics of magnetic environment coupled to superconducting flux qubits. The extracted equilibrium polarization follows Curie-Weiss temperature dependence, suggesting a ferromagnetic phase transition in the system

of environmental spins at a critical temperature $T_c = 5.7 \text{ mK}$. To our knowledge this is the first direct observation of phase transition in the magnetic environment of superconducting devices, although indirect evidences existed before [16]. The measured time dependencies in both the polarization and depolarization experiments are in good agreement with an empirical model that also predicts a noise power spectral density that goes as $1/f^\alpha$ for $\alpha \lesssim 1$. We observe a short and long time cutoffs in the spin bath response at $\sim 10 \mu\text{s}$ and $\sim 4 \text{ ms}$, which correspond to cutoff frequencies $\sim 40 \text{ Hz}$ and $\sim 20 \text{ KHz}$. This suggests deviation from the $1/f^\alpha$ dependence close to those frequencies. An inhomogeneous spin diffusion model with short-time $t^{1/2}$ growth and subsequent stretched-exponential behavior at larger times fits the polarization data up to 1 ms, but deviates after. The observed results agree with spin cluster model of the environment. In this picture, fast spin diffusion dynamics within the clusters are responsible for the short-time (high-frequency) response while the slow fluctuations produce the $1/f^\alpha$ spectrum in the low frequency regime. The latter may be related to the slow evolution of the magnetic moments of the clusters as a whole. More theoretical and experimental investigations are needed to arrive at a more comprehensive model for magnetic flux noise.

Acknowledgements

We thank R. de Sousa and A. Smirnov for fruitful discussion.

Appendix A: Environmental spin polarization

We consider a flux qubit coupled to a spin environment with Hamiltonian (1). It can be shown that the relaxation behavior of $\xi(t)$ is tightly connected to the noise spectral density

$$S_\xi(\omega) = \frac{1}{2} \int_{-\infty}^{\infty} dt e^{i\omega t} \langle \xi(t)\xi(0) + \xi(0)\xi(t) \rangle \quad (A1)$$

through a form of fluctuation dissipation theorem. To see this, let us write the interaction Hamiltonian as

$$\mathcal{H}_{\text{int}}(t) = -\xi(t)b(t) \quad (A2)$$

where b is the force applied to the environmental spins by the qubit, which is proportional to qubit's persistent current. Clearly, $b = \zeta/2$ when the qubit is in classical states with $\sigma_z = \zeta = \pm 1$, and $b = 0$ when the qubit is monostable. Using Kubo formula in linear response theory, we have (herein we assume $\hbar = k_B = 1$)

$$\bar{\xi}(t) = \langle \xi(t) \rangle = i \int_{-\infty}^t dt' \langle [\mathcal{H}_{\text{int}}(t'), \xi(t)] \rangle. \quad (A3)$$

We have assumed that the expectation $\langle \xi(t) \rangle_0$ at $b = 0$ is zero. Introducing retarded Green's function

$$D(t, t') = D(t - t') = i \langle [\xi(t), \xi(t')] \rangle \theta(t - t'), \quad (\text{A4})$$

we obtain

$$\bar{\xi}(t) = \int_{-\infty}^{\infty} dt' D(t - t') b(t'), \quad (\text{A5})$$

where we have used the fact that the noise correlations only depend on $t - t'$. Fourier transformation of this equation yields

$$\bar{\xi}(\omega) = D(\omega) b(\omega), \quad (\text{A6})$$

where

$$D(\omega) = \int_0^{\infty} dt e^{i\omega t} D(t), \quad (\text{A7})$$

is the frequency dependent susceptibility. Notice that we have used $D(t < 0) = 0$. From the fluctuation dissipation theorem, we have

$$S_{\xi}(\omega) = \coth\left(\frac{\omega}{2T}\right) \text{Im} D(\omega) \quad (\text{A8})$$

$$= \coth\left(\frac{\omega}{2T}\right) \int_0^{\infty} dt \sin(\omega t) D(t). \quad (\text{A9})$$

We consider two cases relevant to our experiments: *polarization* and *depolarization*. In polarization, $b = 0$ from $t = -\infty$ to 0 and is switched on at $t = 0$ to $b = \zeta/2$. For $t > 0$, we have

$$\bar{\xi}(t) = -\frac{i\zeta}{2} \int_0^t dt' \langle [\xi(t'), \xi(t)] \rangle \quad (\text{A10})$$

$$= \frac{i\zeta}{2} \int_t^0 d(t - t') \langle [\xi(0), \xi(t - t')] \rangle \quad (\text{A11})$$

$$= \frac{i\zeta}{2} \int_0^t dt' \langle [\xi(t'), \xi(0)] \rangle, \quad (\text{A12})$$

Therefore

$$\frac{d\bar{\xi}(t)}{dt} = \frac{i\zeta}{2} \langle [\xi(t), \xi(0)] \rangle = \frac{\zeta}{2} D(t). \quad (\text{A13})$$

In depolarization, $b = \zeta/2$ from $t = -\infty$ and is switched off at $t = 0$, we obtain

$$\frac{d\bar{\xi}(t)}{dt} = -\frac{\zeta}{2} D(t). \quad (\text{A14})$$

Thus, the relaxation function is closely related to the inverse Fourier transform of the susceptibility.

The fluctuation dissipation theorem, for both polarization and depolarization cases, can now be written as

$$S_{\xi}(\omega) = 2 \coth\left(\frac{\omega}{2T}\right) \int_0^{\infty} dt \sin(\omega t) \left| \frac{d\bar{\xi}(t)}{dt} \right|. \quad (\text{A15})$$

Expressing in terms of flux noise

$$\begin{aligned} S_{\Phi}(\omega) &= \frac{1}{4I_p^2} S_{\xi}(\omega) \\ &= \frac{1}{2I_p^2} \coth\left(\frac{\omega}{2T}\right) \int_0^{\infty} dt \sin(\omega t) \left| \frac{d\bar{\xi}(t)}{dt} \right|. \end{aligned} \quad (\text{A16})$$

In the classical limit $\omega \ll T$, we have

$$S_{\Phi}(\omega) = \frac{T}{\omega I_p^2} \int_0^{\infty} dt \sin(\omega t) \left| \frac{d\bar{\xi}(t)}{dt} \right|. \quad (\text{A17})$$

Note that to obtain $1/\omega$ spectral density, one needs $\bar{\xi}(t) \sim \log t$.

Appendix B: Distribution function of the transient order parameter

If $\mathbf{B}(\mathbf{r})$ represents the magnetic field generated by the qubit at position \mathbf{r} and $\mathbf{M}(\mathbf{r}, t)$ is the magnetization of the environment at the same point and at time t , then

$$\xi(t) = 2\zeta \int d\mathbf{r} \mathbf{B}(\mathbf{r}) \cdot \mathbf{M}(\mathbf{r}, t), \quad (\text{B1})$$

For simplicity, throughout the rest of the paper we only consider $\zeta = +1$. The order parameter ξ is proportional to the flux through the qubit that is generated by the environment: $\xi = 2I_p \delta\Phi_q^{\text{se}}$, where I_p is the qubit's persistent current. In equilibrium, we have $\mathbf{M}(\mathbf{r}, t \rightarrow \infty) = \chi \mathbf{B}(\mathbf{r})$, where χ is the magnetic susceptibility, therefore

$$\bar{\xi}(t \rightarrow \infty) = 2\chi \int d\mathbf{r} \mathbf{B}^2(\mathbf{r}) = \epsilon_p, \quad (\text{B2})$$

where ϵ_p is the equilibrium reorganization energy. To study dynamics of the spin environment, we use Landau-Ginsburg Hamiltonian:

$$\begin{aligned} \mathcal{H}_{en} &= \int d\mathbf{r} [a \mathbf{M}(\mathbf{r}, t)^2 - \mathbf{B}(\mathbf{r}) \cdot \mathbf{M}(\mathbf{r}, t) \\ &\quad + b(\nabla \mathbf{M})^2 + cM^4 + \dots]. \end{aligned} \quad (\text{B3})$$

The coefficient a is related to the static magnetic susceptibility χ as $a = 1/(2\chi)$. Since our primary goal is to describe dynamical effects related to spin diffusion in a paramagnetic phase we may omit the gradient term and various fourth-order terms that are not crucially important for our purpose, and concentrate on a simplified second-order Hamiltonian:

$$\mathcal{H}_{en} = \sum_{\alpha=x,y,z} \int d\mathbf{r} \left[\frac{M_{\alpha}^2(\mathbf{r}, t)}{2\chi} - B_{\alpha}(\mathbf{r}) M_{\alpha}(\mathbf{r}) \right] \quad (\text{B4})$$

Here M_{α} and B_{α} are magnetization and external magnetic field, respectively. We also assume that magnetization is a conserved quantity satisfying the continuity equation:

$$\frac{\partial M_{\alpha}(\mathbf{r}, t)}{\partial t} + \nabla \cdot \mathbf{j}_{\alpha} = 0. \quad (\text{B5})$$

Here \mathbf{j}_α is the magnetization (spin) current, which can be calculated as:

$$\mathbf{j}_\alpha(\mathbf{r}, t) = -\xi \nabla \frac{\delta \mathcal{H}_{en}}{\delta M_\alpha}, \quad (\text{B6})$$

where ξ is the Onsager transport coefficient [21, 22]. Using Eqs. (B4) and Eq. (B6) along with the Einstein relation $\xi = \mathcal{D}\chi$ and substituting Eq. (B6) into (B5) yields the following diffusion equation for the magnetization component $M_\alpha(\mathbf{r}, t)$:

$$\frac{\partial M_\alpha(\mathbf{r}, t)}{\partial t} = \mathcal{D}\nabla^2 [M_\alpha(\mathbf{r}, t) - \chi B_\alpha(\mathbf{r})]. \quad (\text{B7})$$

Suppose we know the eigenfunctions of the stationary diffusion equation (which form coincides with that of the Schrödinger equation)

$$\mathcal{D}\nabla^2 \varphi_n(\mathbf{r}) = -\frac{\varphi_n(\mathbf{r})}{\tau_n}, \quad (\text{B8})$$

where n enumerates diffusion modes. We expand quantities $M_\alpha(\mathbf{r}, t)$ and $B_\alpha(\mathbf{r})$ using the complete set of orthonormal functions $\{\varphi_n(\mathbf{r})\}$:

$$M_\alpha(\mathbf{r}, t) = \sum_n \mu_{\alpha n}(t) \varphi_n(\mathbf{r}), \quad (\text{B9})$$

$$B_\alpha(\mathbf{r}) = \sum_n B_{\alpha n} \varphi_n(\mathbf{r}). \quad (\text{B10})$$

Now we can substitute Eqs. (B9) and (B10) in the diffusion equation (B7) and obtain a set of kinetic (Langevin) equations for each diffusion mode $\mu_{\alpha n}$:

$$\dot{\mu}_{\alpha n} = -\frac{\mu_{\alpha n} - \chi B_{\alpha n}}{\tau_n} + \delta f_{\alpha n}(t), \quad (\text{B11})$$

where $\delta f_{\alpha n}$ is a δ -correlated Gaussian white noise (random force), chosen to ensure the fulfillment of the fluctuation-dissipation theorem. Accordingly, the Hamiltonian in Eq. (B4) can be represented as a sum of the individual-mode Hamiltonians $\mathcal{H}_{en} = \sum_{\alpha n} \mathcal{H}_{\alpha n} - \epsilon_p/2$, where

$$\mathcal{H}_{\alpha n} = \frac{1}{2\chi} (\mu_{\alpha n} - \chi B_{\alpha n})^2 \quad (\text{B12})$$

and

$$\epsilon_p = 2\chi \sum_{\alpha n} B_{\alpha n}^2. \quad (\text{B13})$$

Eqs. (B11) and (B12) resemble Brownian motion of a particle with mass $M = 1/\chi$ moving with velocity $v = \mu_{\alpha n} - \chi B_{\alpha n}$ and having damping (relaxation) rate $\gamma = 1/\tau_n$. We can therefore construct a Fokker-Plank equation for the probability density $P(v, t)$:

$$\frac{\partial P}{\partial t} = \gamma \frac{\partial}{\partial v} \left(vP + \frac{T}{M} \frac{\partial P}{\partial v} \right). \quad (\text{B14})$$

It can be checked (by substitution) that the solution to this equation is

$$P(v, t) = \frac{1}{(2\pi T/M)^{1/2}} \exp \left[-\frac{(v - v_0 e^{-\gamma t})^2}{2T/M} \right], \quad (\text{B15})$$

where v_0 is the expectation of v at $t = 0$.

For the polarization situation where the qubit's persistent current is zero ($B_{\alpha n} = 0$) for $t < 0$ and is turned on at $t = 0$, we have $\langle \mu_{\alpha n} \rangle = 0$, thus, $v_0 = -\chi B_{\alpha n}$. Therefore, for each diffusion mode we have

$$P_n^\alpha(\mu_{\alpha n}, t) = \frac{1}{(2\pi\chi T)^{1/2}} \exp \left[-\frac{(\mu_{\alpha n} - (1 - e^{-t/\tau_n}) B_{\alpha n} \chi)^2}{2\chi T} \right]. \quad (\text{B16})$$

The order parameter (B1) in this representation becomes

$$\xi = 2 \sum_{\alpha n} B_{\alpha n} \mu_{\alpha n} \quad (\text{B17})$$

This allows us to find the probability distribution of ξ as a function of polarization time t :

$$\mathcal{P}(\xi, t) = \int \prod_{\alpha n} d\mu_{\alpha n} \delta \left(\xi - 2 \sum_{\alpha n} B_{\alpha n} \mu_{\alpha n} \right) P_n^\alpha(\mu_{\alpha n}, t) \quad (\text{B18})$$

By using Eq. (B16) we can calculate the multiple Gaussian integral in Eq. (B18) in a standard way as follows. First, we employ the Fourier transform to remove the constraint imposed by the δ -function:

$$\delta \left(\xi - 2 \sum_{\alpha n} B_{\alpha n} \mu_{\alpha n} \right) = \frac{1}{2\pi} \int_{-\infty}^{\infty} dk e^{ik(\xi - 2 \sum_{\alpha n} B_{\alpha n} \mu_{\alpha n})}$$

and then perform series of simple Gaussian integrations to obtain:

$$\mathcal{P}(\xi, t) = \frac{1}{\sqrt{4\epsilon_p T}} \exp \left[-\frac{(\xi - \bar{\xi}(t))^2}{4\epsilon_p T} \right], \quad (\text{B19})$$

where

$$\begin{aligned} \bar{\xi}(t) &= 2\chi \sum_{\alpha n} B_{\alpha n}^2 \left(1 - e^{-t/\tau_n} \right) \\ &= \epsilon_p \left[1 - \sum_n p_n e^{-t/\tau_n} \right], \end{aligned} \quad (\text{B20})$$

is the ensemble average of ξ at time t , ϵ_p is the reorganization energy given by Eq. (B13), and $p_n = \sum_\alpha B_{\alpha n}^2 / \sum_{\alpha, n} B_{\alpha n}^2$ measures the relative contribution of the n th diffusion mode in the relaxation process.

For the case of depolarization, the qubit's persistent current is nonzero for $t < 0$ and is turned off at $t = 0$ by making the qubit monostable. The environment is therefore polarized to $\mu_{\alpha n}^0$ leading to the initial value of the order parameter

$$\bar{\xi}(0) = 2 \sum_{\alpha n} B_{\alpha n} \mu_{\alpha n}^0. \quad (\text{B21})$$

If the polarization time is t_0 , then $\mu_{\alpha n}^0 = \chi B_{\alpha n}(1 - e^{-t_0/\tau_n})$. At $t > 0$, qubit persistent current is absent, hence $B_{\alpha n} = 0$. The initial velocity in Eq. (B15) is therefore $v_0 = \mu_{\alpha n}^0$, leading to

$$P_n^\alpha(\mu_{\alpha n}, t) = \frac{1}{(2\pi\chi T)^{1/2}} \exp\left[-\frac{(\mu_{\alpha n} - \mu_{\alpha n}^0 e^{-t/\tau_n})^2}{2\chi T}\right]. \quad (\text{B22})$$

The order parameter $\bar{\xi}(t)$ is defined in the bistable state of the qubit according to (1). We therefore use (B17) for its definition, keeping in mind that $B_{\alpha n}$ correspond to the bistable state of the qubit. In other word, $\bar{\xi}(t)$ is the energy bias the qubit would experience if it becomes bistable at time t . The probability distribution of ξ is again given by (B18) with $P_n^\alpha(\mu_{\alpha n}, t)$ defined in Eq. (B22). Following the same calculations as before, we arrive at (B19) with

$$\begin{aligned} \bar{\xi}(t) &= 2 \sum_{\alpha n} B_{\alpha n} \mu_{\alpha n}^0 e^{-t/\tau_n} \\ &= 2\chi \sum_{\alpha n} B_{\alpha n}^2 (1 - e^{-t_0/\tau_n}) e^{-t/\tau_n} \\ &= \epsilon_p \sum_{\alpha n} p_n [e^{-t/\tau_n} - e^{-(t+t_0)/\tau_n}] \end{aligned} \quad (\text{B23})$$

Equations (B20) and (B23) can be written as

$$\bar{\xi}(t) = \epsilon_p [1 - F(t)], \quad (\text{B24})$$

for polarization, and

$$\bar{\xi}(t) = \epsilon_p [F(t) - F(t+t_0)]. \quad (\text{B25})$$

for depolarization, where t_0 is the polarization time during the polarization process and

$$F(t) = \sum_n p_n e^{-t/\tau_n}. \quad (\text{B26})$$

Notice that $F(0) = 1$ and $F(\infty) = 0$. Therefore, the initial polarization in (B25) is $\bar{\xi}(0) = \epsilon_p [1 - F(t_0)]$, in agreement with t_0 being the polarization time. Equations (B19)-(B25), although derived for the fluctuations of spin diffusion modes, hold for any set of independent fluctuators following Langevin dynamics.

Substituting Eq. (B20) or (B23) into Eq. (A17), we obtain

$$\begin{aligned} S_\Phi(\omega) &= \frac{\epsilon_p T}{\omega I_p^2} \int_0^\infty dt \sin(\omega t) \sum_n \frac{p_n}{\tau_n} e^{-t/\tau_n} \\ &= \frac{\epsilon_p T}{\omega I_p^2} \sum_n \frac{p_n}{\tau_n} \int_0^\infty dt \sin(\omega t) e^{-t/\tau_n} \\ &= \frac{\epsilon_p T}{I_p^2} \sum_n \frac{p_n \tau_n}{\omega^2 \tau_n^2 + 1}. \end{aligned} \quad (\text{B27})$$

One may also take the continuous- τ limit of (B27) by replacing p_n with the distribution $p(\tau)$:

$$S_\Phi(\omega) = \frac{\epsilon_p T}{I_p^2} \int_0^\infty d\tau \frac{p(\tau)\tau}{\omega^2 \tau^2 + 1}. \quad (\text{B28})$$

We now derive $F(t)$ for a few different models. For simplicity, we only consider polarization cases in detail.

Appendix C: $1/f^\alpha$ -noise model

To achieve $1/f^\alpha$ noise spectrum, we need

$$p(\tau) = \begin{cases} \mathcal{N} \tau^{\alpha-2} & \tau_{\min} < \tau < \tau_{\max} \\ 0 & \text{otherwise} \end{cases} \quad (\text{C1})$$

where

$$\mathcal{N}^{-1} = \begin{cases} \log(\tau_{\max}/\tau_{\min}) & \alpha = 1 \\ (\alpha-1)^{-1} [\tau_{\max}^{\alpha-1} - \tau_{\min}^{\alpha-1}] & \alpha \neq 1 \end{cases} \quad (\text{C2})$$

is a normalization factor. Substituting (C1) into (B27), we find $S_\Phi(\omega) \sim \omega^{-\alpha}$ for $\tau_{\max}^{-1} < \omega < \tau_{\min}^{-1}$. Also, from (B26), we obtain

$$\begin{aligned} F(t) &= \int_0^\infty d\tau p(\tau) e^{-t/\tau} \\ &= \mathcal{N} \int_{\tau_{\min}}^{\tau_{\max}} d\tau \tau^{\alpha-2} e^{-t/\tau} \\ &= \mathcal{N} t^{\alpha-1} \int_{t/\tau_{\max}}^{t/\tau_{\min}} du u^{-\alpha} e^{-u} \\ &= \mathcal{N} t^{\alpha-1} [\Gamma(1-\alpha, t/\tau_{\max}) - \Gamma(1-\alpha, t/\tau_{\min})]. \end{aligned} \quad (\text{C3})$$

where

$$\Gamma(s, x) = \int_x^\infty t^{s-1} e^{-t} dt \quad (\text{C4})$$

is the incomplete gamma-function.

Appendix D: Spin diffusion model

We now move to more elaborate theories based on spin diffusion. Consider the simplest case of environmental spins in a thin wire of length L and width W . We neglect the height of the wire and assume that the flux noise is produced by environmental spins on the 2D interface of the wire. If x and z represent directions along the width and length of the wire respectively, the magnetic field generated by the persistent current, $B(x)$, will only be a function of x and independent of z . The behavior of the homogeneous system is therefore effectively 1D. We can therefore calculate the contribution of a narrow region with width dz to the order parameter and then add them up. Such a narrow region would essentially behave like a spin chain. We consider the homogeneous spin diffusion model as a special case of the inhomogeneous model, where only one length scale is associated with all chains. For the inhomogeneous case, we assume there are vacancies (defects) that break the chain into smaller 1D regions of length w_i , with $\sum_i w_i = W$.

For the i th region, the solutions, $\varphi_n(x)$, to Eq. (B8) are Fourier terms $\sin k_n x$ and $\cos k_n x$, with $k_n = 2\pi n/w_i$ and $\tau_n^{-1} = \gamma_n = \mathcal{D}k_n^2$. We can approximate the magnetic field in the i th segment

$$B(x) = \bar{B}_i + B'_i x, \quad -w_i/2 \leq x \leq w_i/2, \quad (\text{D1})$$

where \bar{B}_i is the average magnetic field and $B'_i = (\partial B/\partial x)_0$. Fourier expansion of B is given by

$$B(x) - \bar{B}_i = \sqrt{\frac{2}{w_i}} \sum_{n=1}^{\infty} B_n^i \sin k_n x \quad (\text{D2})$$

where the cosine terms are absent by construction and the form-factors B_n^i can be expressed as:

$$\begin{aligned} B_n^i &= \sqrt{\frac{2}{w_i}} \int_{-w_i/2}^{w_i/2} dx B(x) \sin k_n x \\ &= B'_i \frac{(-1)^{n+1} \sqrt{2w_i}}{k_n}. \end{aligned} \quad (\text{D3})$$

The magnetization is also independent of z and similar to $B(x)$ has the Fourier expansion

$$M(x, t) = \sqrt{\frac{2}{w_i}} \sum_{n=1}^{\infty} \mu_n(t) \sin k_n x. \quad (\text{D4})$$

Notably, the term with $n = 0$ is absent in Eq. (D4). This is because the total magnetization is a conserved quantity and is assumed to be zero ($\int dx M(x, t) = 0$) before the magnetic field was turned on, in the polarization case, and will remain zero despite the presence of \bar{B} . If the only relaxation mechanism in the system is spin diffusion the total magnetic moment will remain zero although the local magnetization will be induced by the nonuniform components of the magnetic field. Uniform magnetic field may induce magnetization only in the presence of some local relaxation mechanism, e.g., spin-phonon relaxation.

We can now calculate contribution of this region to the order parameter. From (B20), we have

$$\begin{aligned} d\bar{\xi}_i(t) &= 2dz \int dx B(x) M(x, t) \\ &= 2dz \chi \sum_{n=1}^{\infty} B_n^{i2} (1 - e^{-t/\tau_n}), \end{aligned} \quad (\text{D5})$$

where $\tau_n^{-1} = \mathcal{D} (2\pi n/w_i)^2$. Substituting B_n^i by (D3), we obtain

$$d\bar{\xi}_i(t) = dz \chi B_i'^2 \sum_{n=1}^{\infty} \frac{w_i^3}{\pi^2 n^2} (1 - e^{-\mathcal{D}(2\pi n/w_i)^2 t}). \quad (\text{D6})$$

Assuming that the size of clusters are distributed according to the distribution $P(w)$, the order parameter is given by

$$\begin{aligned} \bar{\xi}(t) &= L \chi \sum_i B_i'^2 \sum_{n=0}^{\infty} \int_0^{\infty} dw P(w) \\ &\quad \times \frac{w^3}{\pi^2 n^2} \left[1 - e^{-\mathcal{D}(2\pi n/w)^2 t} \right]. \end{aligned} \quad (\text{D7})$$

We now need to find $P(w)$, which we shall do for both inhomogeneous and homogeneous cases.

1. Inhomogeneous case

Let η be the linear density of defects. For a region of length w , the average number of defect is ηw . The probability of having k defects within this region is given by Poisson distribution: $e^{-\eta w} (\eta w)^k / k!$, hence the probability of this region being defect-free ($k = 0$) is $e^{-\eta w}$. The distribution of w is therefore given by the normalized probability density

$$P(w) = \bar{w}^{-1} e^{-w/\bar{w}}, \quad (\text{D8})$$

where $\bar{w} = \eta^{-1}$ is the average length of the clusters. The expected contribution of a region can be calculated by integrating (D6) over all w with the above distribution. Summing over the whole wire, we obtain

$$\begin{aligned} \bar{\xi}(t) &= L \chi \sum_i B_i'^2 \sum_{n=0}^{\infty} \int_0^{\infty} \frac{dw}{\bar{w} \pi^2 n^2} e^{-w/\bar{w}} \\ &\quad \times w^3 \left[1 - e^{-\mathcal{D}(2\pi n/w)^2 t} \right]. \end{aligned} \quad (\text{D9})$$

To evaluate the sum in Eq. (D9) we change the variables in each term of the series by replacing w with $2n\bar{w}v$ and interchanging the order of summation and integration. This yields:

$$\bar{\xi}(t) = \frac{16L\bar{w}^3 \chi}{\pi^2} \sum_i B_i'^2 \int_0^{\infty} dv v^3 \left(1 - e^{-\Omega t/v^2} \right) \sum_{n=0}^{\infty} n^2 e^{-2nv} \quad (\text{D10})$$

where $\Omega = \pi^2 \mathcal{D} / \bar{w}^2$. Note that $\sqrt{\mathcal{D}t}$ is the length over which spin diffusion happens after time t , therefore Ω^{-1} is the timescale for diffusion to reach the length \bar{w} . Calculating the sum in Eq. (D10) is straightforward and we finally obtain

$$\bar{\xi}(t) = \epsilon_p [1 - F(t)], \quad (\text{D11})$$

where $\epsilon_p = L\bar{w}^3 \chi \sum_i B_i'^2$ and

$$F(t) = \frac{4}{\pi^2} \int_0^{\infty} dv v^3 \frac{\coth(v)}{\sinh^2(v)} e^{-\Omega t/v^2}. \quad (\text{D12})$$

Note that $F(0) = 1$ and $F(\infty) = 0$. Therefore, $\bar{\xi}(\infty) = \epsilon_p$, as expected.

The noise spectral density based on this model is

$$\begin{aligned} S_{\Phi}(\omega) &= \frac{T}{\omega I_p^2} \int_0^{\infty} dt \sin(\omega t) \left| \frac{d\bar{\xi}(t)}{dt} \right| \\ &= \frac{4\Omega T \epsilon_p}{\omega \pi^2 I_p^2} \int_0^{\infty} dv v \frac{\coth(v)}{\sinh^2(v)} \int_0^{\infty} dt \sin(\omega t) e^{-\Omega t/v^2} \\ &= \frac{4T \epsilon_p}{\Omega \pi^2 I_p^2} \int_0^{\infty} dv \frac{\coth(v)}{\sinh^2(v)} \frac{v}{(\omega/\Omega)^2 + v^{-4}}. \end{aligned} \quad (\text{D13})$$

It is instructive to investigate the short and long-time asymptotics of $\bar{\xi}(t)$. For $\Omega t \ll 1$, or equivalently $\sqrt{\mathcal{D}t} \ll \bar{w}$, we consider

$$1 - F(t) = \frac{4}{\pi^2} \int_0^\infty dv v^3 \frac{\coth(v)}{\sinh^2(v)} (1 - e^{-\Omega t/v^2}), \quad (\text{D14})$$

which is well behaved in both small and large v integration limits. The dominant contribution to the integral comes from small v regions, for which we can approximately write

$$\frac{\coth(v)}{\sinh^2(v)} \approx v^{-3}. \quad (\text{D15})$$

Substituting back and changing the integration variable to $u = K/v$, we obtain

$$1 - F(t) = \frac{4\sqrt{\Omega t}}{\pi^2} \int_0^\infty \frac{du}{u^2} (1 - e^{-u^2}) = \frac{16\sqrt{\Omega t}}{\pi^{7/2}}. \quad (\text{D16})$$

Therefore,

$$F(t) \approx 1 - C\sqrt{\Omega t}, \quad (\text{D17})$$

where $C = 16\pi^{-7/2}$. This means for short times $\bar{\xi}(t) \sim \sqrt{t}$, similar to the homogeneous case discussed in the next subsection. The reason is when the spin diffusion length, $\sqrt{\mathcal{D}t}$, is much smaller than the average length of the clusters, \bar{w} , disorder is effectively invisible to the diffusion process and the system should behave similar to a homogeneous spin system.

When $\Omega t \gg 1$, the integral in (D12) is dominated by large v regions. We can therefore substitute

$$\frac{\coth(v)}{\sinh^2(v)} \approx 4e^{-2v} \quad (\text{D18})$$

into (D12) to obtain

$$F(t) = \frac{16}{\pi^2} \int_0^\infty dv v^3 e^{-2v - \Omega t/v^2}. \quad (\text{D19})$$

The integrand is sharply peaked near $v_0 = (\Omega t)^{1/3}$. Using the steepest descent method, we substitute $v = v_0$ in the exponent to obtain

$$F(t) \sim e^{-3v_0} = e^{-3(\Omega t)^{1/3}}. \quad (\text{D20})$$

The timescale Ω^{-1} is the time needed for spin polarization to diffuse over a length of the order of the average size of the clusters, \bar{w} . The short and long-time asymptotic behavior of $F(t)$ can therefore be summarized by

$$F(t) = \begin{cases} 1 - C\sqrt{\Omega t} & \text{for } t \ll \Omega^{-1} \\ C'e^{-3(\Omega t)^{1/3}} & \text{for } t \gg \Omega^{-1} \end{cases}. \quad (\text{D21})$$

2. Homogeneous case

In the homogeneous case, there is only one length scale \bar{w} for all chains, determined by the geometry. Therefore

$$P(w) = \delta(w - \bar{w}), \quad (\text{D22})$$

where $\bar{w} = O(W)$, with W being the width of the wire. Substituting into (D7), we obtain

$$\bar{\xi}(t) = L\chi B'^2 \sum_{n=0}^\infty \frac{\bar{w}^3}{\pi^2 n^2} \left[1 - e^{-\mathcal{D}(2\pi n/\bar{w})^2 t} \right]. \quad (\text{D23})$$

Using $\bar{\xi}(t \rightarrow \infty) = \epsilon_p$, we have

$$\epsilon_p = L\chi B'^2 \frac{\bar{w}^3}{\pi^2} \sum_{n=1}^\infty \frac{1}{n^2} = \frac{1}{6} L\chi B'^2 \bar{w}^3. \quad (\text{D24})$$

Therefore, (D23) can be written as

$$\bar{\xi}(t) = \epsilon_p [1 - F(t)], \quad (\text{D25})$$

where

$$F(t) = \frac{6}{\pi^2} \sum_{n=1}^\infty \frac{e^{-4(\Omega t)n^2}}{n^2}, \quad (\text{D26})$$

with $\Omega = \mathcal{D}(\pi/\bar{w})^2$, defined the same as in the inhomogeneous case.

We can now find the short- and long-time asymptotic behavior of $F(t)$. For long timescales, only $n = 1$ survives in the exponential of (D25). Hence

$$F(t) = C'e^{-4\Omega t}, \quad (\text{D27})$$

where $C' = 6\pi^{-2}$. For short timescales we can replace the sum with an integral

$$1 - F(t) = \frac{6}{\pi^2} \int_0^\infty \frac{dv}{v^2} \left[1 - e^{-4\Omega t v^2} \right] \quad (\text{D28})$$

Changing the integration variable to $u = 2\sqrt{\Omega t} v$, we obtain

$$\begin{aligned} 1 - F(t) &= \frac{6}{\pi^2} \sqrt{\Omega t} \int_0^\infty \frac{du}{u^2} \left[1 - e^{-u^2} \right] \\ &= \frac{48}{\pi^{7/2}} \sqrt{\Omega t}. \end{aligned} \quad (\text{D29})$$

The short- and long-time asymptotic behavior of $F(t)$ can therefore be summarized by

$$F(t) = \begin{cases} 1 - C\sqrt{\Omega t} & \text{for } t \ll \Omega^{-1} \\ C'e^{-4\Omega t} & \text{for } t \gg \Omega^{-1} \end{cases}, \quad (\text{D30})$$

where $C = 48\pi^{-7/2}$ and $C' = 6\pi^{-2}$. The \sqrt{t} dependence at short times leads to $S_\Phi(\omega) \sim \omega^{-3/2}$ at large frequencies, above $f_c \sim W^2/\mathcal{D}$, in agreement with the numerical calculations in Ref. [11]. The crossover frequency in Ref. [11] is 0.1-1 Hz, which means the \sqrt{t} dependence is expected to continue up to 1-10 s.

-
- [1] G. Wendin, Reports on Progress in Physics **80**, 106001 (2017).
- [2] J. Clarke, W. M. Goubau, and M. B. Ketchen, Journal of Low Temperature Physics **25**, 99 (1976).
- [3] R. H. Koch, J. Clarke, W. Goubau, J. M. Martinis, C. Pegrum, and D. J. Van Harlingen, Journal of low temperature physics **51**, 207 (1983).
- [4] F. C. Wellstood, C. Urbina, and J. Clarke, Applied Physics Letters **50**, 772 (1987).
- [5] F. Yoshihara, K. Harrabi, A. O. Niskanen, Y. Nakamura, and J. S. Tsai, Phys. Rev. Lett. **97**, 167001 (2006).
- [6] T. Lanting, A. J. Berkley, B. Bumble, P. Bunyk, A. Fung, J. Johansson, A. Kaul, A. Kleinsasser, E. Ladizinsky, F. Maibaum, et al., Phys. Rev. B **79**, 060509 (2009).
- [7] R. C. Bialczak, R. McDermott, M. Ansmann, M. Hofheinz, N. Katz, E. Lucero, M. Neeley, A. D. O'Connell, H. Wang, A. N. Cleland, et al., Phys. Rev. Lett. **99**, 187006 (2007).
- [8] R. H. Koch, D. P. DiVincenzo, and J. Clarke, Phys. Rev. Lett. **98**, 267003 (2007).
- [9] R. De Sousa, Physical Review B **76**, 245306 (2007).
- [10] L. Faoro and L. B. Ioffe, Phys. Rev. Lett. **100**, 227005 (2008).
- [11] T. Lanting, M. H. Amin, A. J. Berkley, C. Rich, S. F. Chen, S. LaForest, and R. de Sousa, Phys. Rev. B **89**, 014503 (2014).
- [12] K. Kechedzhi, L. Faoro, and L. B. Ioffe, arXiv preprint arXiv:1102.3445 (2011).
- [13] A. De, Phys. Rev. Lett. **113**, 217002 (2014).
- [14] A. De, Phys. Rev. B **99**, 024305 (2019).
- [15] S. LaForest and R. de Sousa, Phys. Rev. B **92**, 054502 (2015).
- [16] S. Sendelbach, D. Hover, A. Kittel, M. Mück, J. M. Martinis, and R. McDermott, Phys. Rev. Lett. **100**, 227006 (2008).
- [17] R. Harris, J. Johansson, A. J. Berkley, M. W. Johnson, T. Lanting, S. Han, P. Bunyk, E. Ladizinsky, T. Oh, I. Perminov, et al., Phys. Rev. B **81**, 134510 (2010).
- [18] S. Kogan, *Electronic Noise and Fluctuations in Solids* (Cambridge University Press, Cambridge, 1996).
- [19] P. Kopietz, Phys. Rev. B **57**, 7829 (1998).
- [20] J. D. Jackson, *Classical electrodynamics* (Wiley, New York, NY, 1999).
- [21] H. S. Bennett and P. C. Martin, Phys. Rev. **138**, A608 (1965).
- [22] P. M. Chaikin and T. C. Lubensky, *Principles of condensed matter physics* (Cambridge University Press, Cambridge, 2009).
- [23] A simple exponential function, $F(t) = e^{-\gamma t}$, gives the expected exponential growth, $\bar{\xi}(\tau_p) = \epsilon_p(1 - e^{-\gamma\tau_p})$, and exponential decay $\bar{\xi}(\tau_d) = \bar{\xi}(0)e^{-\gamma\tau_d}$, but Eq. (3) holds for any other functional form.